On shape optimization with stochastic loadings

Pradeep Atwal, Sergio Conti, Benedict Geihe, Martin Pach, Martin Rumpf and Rüdiger Schultz

Abstract. This article is concerned with different approaches to elastic shape optimization under stochastic loading. The underlying stochastic optimization strategy builds upon the methodology of two-stage stochastic programming. In fact, in the case of linear elasticity and quadratic objective functional our strategy leads to a computational cost which scales linearly in the number of *linearly independent* applied forces, even for a large set of realization of the random loading. We consider, besides minimization of the expectation value of suitable objective functionals, also two different risk-averse approaches, namely the *expected excess* and the *excess probability*. Numerical computations are performed using either a level-set approach representing implicit shapes of general topology in combination with composite finite elements to resolve elasticity in two and three dimensions, or a collocation boundary element approach, where polygonal shapes represent geometric details attached to a lattice and describing a perforated elastic domain. Topology optimization is performed using the concept of topological derivatives. We generalize this concept, and derive an analytical expression which takes into account the interaction between neighboring holes. This is expected to allow efficient and reliable optimization strategies of elastic objects with a large number of geometries details on a fine scale.

Mathematics Subject Classification (2000). 90C15, 74B05, 65N30, 65N38, 34E08, 49K45.

Keywords. shape optimization in elasticity, two-stage stochastic programming, risk averse optimization, level set method, boundary element method, topological derivative.

1. Introduction

Data uncertainty is a critical feature of many real-world shape optimization problems. When optimizing elastic structures, it has to be taken into account that volume and in particular surface loadings typically vary over time. Often, these variations can be captured by probability distributions. In order to study the resulting random optimization problem it is crucial to observe that decisions on the shape must be nonanticipative, *i. e.*, be made before applying the stochastic forcing. In terms of optimization this implies that, for a fixed candidate shape, each realization of the stochastic force determines a value of the optimality criterion. Hence, the shape is assigned a random variable whose realizations are the values of the optimality criterion induced by the data realizations.

From this point of view, shape optimization under (stochastic) uncertainty amounts to finding "optimal" shapes in sets of random variable shapes. The quotes shall indicate that different concepts for ranking random variables may apply. In the present paper we discuss risk neutral as well as risk averse models. While in the former the ranking is done by comparing the expectation values, in the latter statistical parameters reflecting different perceptions of risk are applied. This bears striking conceptual similarity with finite-dimensional two-stage stochastic programming.

The paper is organized as follows. After a brief review of related work in Section 2, we introduce in Section 3 the elastic state equation, define suitable cost functionals, and formulate an initial random shape optimization model with stochastic loading. Starting from basic paradigms of finite dimensional two-stage stochastic programming, Section 4 serves to introduce general classes of risk-neutral and risk-averse shape-optimization models. Computation of shape derivatives is

addressed in Section 5. In Section 6 we present our methods for describing shapes, namely, the level-set approach and parametrized perforated domains. Section 7 describes our numerical algorithms. A selection of case studies is presented in Section 8, to demonstrate the validity of our conceptual approach and the effectiveness of the algorithm. Section 9 discusses a new analytical result on the hole-hole interaction in topological derivatives, and outlines its possible application to a reduced model for the optimization of perforated geometries.

2. Related work

Deterministic shape optimization. Shape optimization under deterministic loading is a well-developed field within PDE-constrained optimization; see for example the books [62, 16, 3]. We shall not review here the details, simply remark that the usual strategy of performing iteratively modifications of the boundary, following the shape derivative, does not permit to optimize the topology of the shape, and that the homogenization strategy delivers shapes with microstructures at many different scales, which may be difficult to realize in practice.

Topology optimization. The optimal shape determined using the shape derivative alone may strongly depend on this choice of the initial topology (cf. [5, 8, 25]). This is not only due to the discretization, but also to the descent strategy itself. Indeed, even with a level-set description which in principle entails no restriction on the topology, the evolution of a level set based on a gradient flow is able to merge existing holes, but not capable of creating new holes. The possibility of creating new holes is the key idea behind the so-called "bubble method" or *topological sensitivity*. The method is based on considering variations of the domain corresponding to the insertion of small holes of prescribed shape and computing an asymptotic expansion depending on the radius ρ. After its introduction by Schumacher [53], the method was generalized to a wider class of shape functionals by Sokołowski and Żokowski [59] and applied to 3D elasticity in [60]. In [61], the approach is extended to the case of finitely many circular holes, combining topology variations with boundary variations simultaneously. Using an adjoint method and a truncation technique, Garreau et al. [31] computed the topological sensitivity for general objective functionals and arbitrarily-shaped holes. The topological derivative has been incorporated into the level set method, e.g. in [17], and also combined with the shape derivative in that context (cf. e.g. [5, 10, 35]). The topological derivative permits arbitrary changes in the topology, but remains a local modification. In particular, even in this case there is no guarantee to reach the global minimum, although one produces a local minimum which is stable under a wider class of variations and includes in particular topology changes (cf. Fig. 14).

Finite dimensional stochastic programming. The principal modeling approaches in optimization under uncertainty differ in their requirements on data information. Worst-case models, as in online or robust optimization [2, 14], merely ask for ranges of the uncertain parameters. Applications to shape optimization can be found in [12, 36, 26, 21, 20]. In stochastic optimization, see [56] for a recent textbook, data uncertainty is captured by probability distributions. In finite dimension, there exists a rich theory and methodology of linear models [49, 56] and, to lesser extent, linear mixed-integer or nonlinear models [13, 46, 50, 63]. Stochastic optimization in continuous time has been analyzed in stochastic dynamic programming and stochastic control, see [30, 19]. Stochastic shape optimization in the design of mechanical or aerodynamic structures, has been addressed in [40, 52]. The difference of these contributions to the present paper is in the decision spaces. In [40, 52] these are Euclidean spaces, while our design decisions are allowed to be shapes (open sets) in suitable working domains.

Multiload shape optimization. Most shape-optimization approaches are based on considering one given, typical, load configuration. This is not always realistic, and indeed multiload approaches have been developed, in which a fixed (usually small) number of different loading configurations is considered and optimization refers to this set of configurations, see, e.g., [6, 32, 66, 11] and references therein. These approaches are based on evaluating the objective functional separately for each of the possible values of the loading, which renders them infeasible if the set of possible forces is large, as for example is the case when one aims at approximating a continuous distribution of forces. In case of additional geometrical assumptions a more efficient method was derived in [9], where optimization of the expected compliance is shown to be equivalent to a convex problem, and hence efficiently solvable. Our approach is instead based on the solution of the elasticity PDE

only for the basis modes for the surface and volume loading. Additionally, besides an optimization of the expected value of the cost we investigate also the optimization of nonlinear risk measures acting on the cost functional. A robust probabilistic approach for the optimization of simple beam models is discussed in [1], whereas in [41] structural reliability is discussed for beam geometries with uncertain load magnitude. Worst-case situations in a multiload context have also been considered, see, e.g., [15]. Structural optimization under incomplete information is also addressed in [12]. The authors investigate different types of uncertainties and follow a non-probabilistic, robust worst case approach. They work out effective techniques to transform optimal design problems with uncertainties into conventional structural optimization problems. In [48] a worst case analysis for given bounds on uncertain loads has been implemented based on a boundary element approach. A worst case compliance optimization is investigated in [7] based on a level set description of shapes and a semi–definite programming approach in the minimization algorithm. Schulz et al. [52] discussed shape optimization under uncertainty in aerodynamic design. Uncertainty is captured by Euclidean parameters following truncated normal distributions and leading to optimization models of the type of finite dimensional nonlinear programs. Due to the distributional assumptions, there are explicit formulas for relevant probability functionals.

3. Shape Optimization Model with Linear Elasticity and Random Loading

The state equation. For a fixed elastic domain $\mathcal{O}$ and given stochastic loading we take into account linearized elasticity to determine a displacement $u : \mathcal{O} \to \mathbb{R}^d$ as the elastic response to applied forces. Hereby, we assume $\mathcal{O}$ to be a sufficiently regular subset of a fixed, bounded working domain $D \subset \mathbb{R}^d$. The boundary of $\mathcal{O}$ is assumed to be decomposed into a Dirichlet boundary Γ_D on which we prescribe homogeneous Dirichlet boundary conditions $u = 0$, a Neumann boundary Γ_N on which the surface loading is applied, and the remaining homogeneous Neumann boundary $\partial\mathcal{O} \setminus (\Gamma_D \cup \Gamma_N)$, those shape is to be optimized according to some objective functional, to be discussed later. Neither Γ_D nor Γ_N will be subject to the shape optimization. For details on the concrete handling of the boundary conditions in the shape optimization we refer to [25]. Concerning the loading, we are in particular interested in a stochastic loads. Thus, we assume a random volume force $f(\omega) \in L^2(D; \mathbb{R}^d)$ and a random surface force $g(\omega) \in L^2(\Gamma_N; \mathbb{R}^d)$ to be given. Here ω denotes a realization on a probability space Ω. Based on this setup u is given as the solution of the following elliptic boundary value problem of linearized elasticity

$$
\begin{aligned}
-\operatorname{div}(\mathbf{C}\varepsilon(u)) &= f(\omega) & &\text{in } \mathcal{O}\,, \\
u &= 0 & &\text{on } \Gamma_D\,, \\
(\mathbf{C}\varepsilon(u))n &= g(\omega) & &\text{on } \Gamma_N\,, \\
(\mathbf{C}\varepsilon(u))n &= 0 & &\text{on } \partial\mathcal{O} \setminus \Gamma_N \setminus \Gamma_D\,.
\end{aligned}
\tag{1}
$$

Here, $\varepsilon(u) = \frac{1}{2}(\nabla u + \nabla u^\top)$ is the linearized strain tensor and $\mathbf{C} = (\mathbf{C}_{ijkl})_{ijkl}$ denotes the elasticity tensor. For the sake of simplicity, we restrict ourselves here to isotropic materials, *i. e.* $\mathbf{C}_{ijkl} = 2\mu\delta_{ik}\delta_{jl} + \lambda\delta_{ij}\delta_{kl}$, where δ_{ij} denotes the Kronecker symbol and μ, λ the positive Lamé constants of the material. For any open, connected set $\mathcal{O}$ with Lipschitz boundary and any fixed realization ω of the random loading, there exists a unique weak solution $u = u(\mathcal{O}, \omega) \in H^1(\mathcal{O}; \mathbb{R}^d)$ of (1) [22, 39]. This solution can equivalently be characterized as the unique minimizer of the quadratic functional

$$
E(\mathcal{O}, u, \omega) \quad := \quad \frac{1}{2}a(\mathcal{O}, u, u) - l(\mathcal{O}, u, \omega) \quad \text{with}
\tag{2}
$$

$$
a(\mathcal{O}, \psi, \theta) \quad := \quad \int_{\mathcal{O}} \mathbf{C}_{ijkl}\varepsilon_{ij}(\psi)\varepsilon_{kl}(\theta)\,\mathrm{d}x\,,
\tag{3}
$$

$$
l(\mathcal{O}, \theta, \omega) \quad := \quad \int_{\mathcal{O}} f_i(\omega)\theta_i\,\mathrm{d}x + \int_{\Gamma_N} g_i(\omega)\theta_i\,\mathrm{d}\mathcal{H}^{d-1}
\tag{4}
$$

on $H^1_{\Gamma_D}(\mathcal{O}; \mathbb{R}^d):=\{u \in H^1(\mathcal{O}; \mathbb{R}^d)\,|\, u = 0 \text{ on } \Gamma_D \text{ in the sense of traces}\}$. Here and below, we use the summation convention and implicitly sum over repeated indices.

The random shape optimization model. Next, we fomulate the actual shape optimization problem and take into account an objective functional J which depends on both the shape $\mathcal{O}$ and the resulting elastic displacement $u(\mathcal{O}, \omega)$. Let us assume that J is of the form

$$J(\mathcal{O}, \omega) = \int_{\mathcal{O}} j\left(u\left(\mathcal{O}, \omega\right)\right) \,\mathrm{d}x + \int_{\Gamma_N} k\left(u\left(\mathcal{O}, \omega\right)\right) \,\mathrm{d}\mathcal{H}^{d-1} \,. \tag{5}$$

To allow for a subsequent efficient numerical realization in the context of a high number of stochastic scenarios of the loading we confine ourselves to linear or quadratic functions $j(.)$ and $k(.)$. Finally, we obtain the random shape optimization model with stochastic loading

$$\min\left\{J\left(\mathcal{O}, \omega\right) : \mathcal{O} \in \mathcal{U}_{\mathrm{ad}}\right\} \tag{6}$$

where $\mathcal{U}_{\mathrm{ad}}$ is a suitable set of admissible shapes. The potential energy of the applied loading for given displacement

$$J_1\left(\mathcal{O}, \omega\right) := \int_{\mathcal{O}} f \cdot u(\mathcal{O}, \omega) \,\mathrm{d}x + \int_{\Gamma_N} g \cdot u(\mathcal{O}, \omega) \,\mathrm{d}\mathcal{H}^{d-1} \,, \tag{7}$$

which is denoted the compliance, is the most common objective functional, which we pick up here also in the stochastic context. Alternatively, one might consider the least square error compared to a target displacement u_0

$$J_2\left(\mathcal{O}, \omega\right) := \frac{1}{2} \int_{\mathcal{O}} \left|u\left(\mathcal{O}, \omega\right) - u_0\right|^2 \,\mathrm{d}x \,. \tag{8}$$

or alternatively

$$J_3\left(\mathcal{O}, \omega\right) := \frac{1}{2} \int_{\partial\mathcal{O}} \left|u\left(\mathcal{O}, \omega\right) - u_0\right|^2 \,\mathrm{d}\mathcal{H}^{d-1} \,, \tag{9}$$

which is used in the context of parametrized perforated domains (8). For the level approach we usually include in the objective functional a penalty for the object volume $\alpha \int_{\mathcal{O}} \mathrm{d}x$ with $\alpha \geq 0$. Having defined the objective functional we are in a position to consider the optimization of the shape with respect to a fixed realization of the randomness. Starting from this deterministic case we will then introduce general classes of risk-neutral (cf. Fig. 1) and risk-averse stochastic cost functionals, where a different (nonlinear) weighting is applied on the probability space Ω.
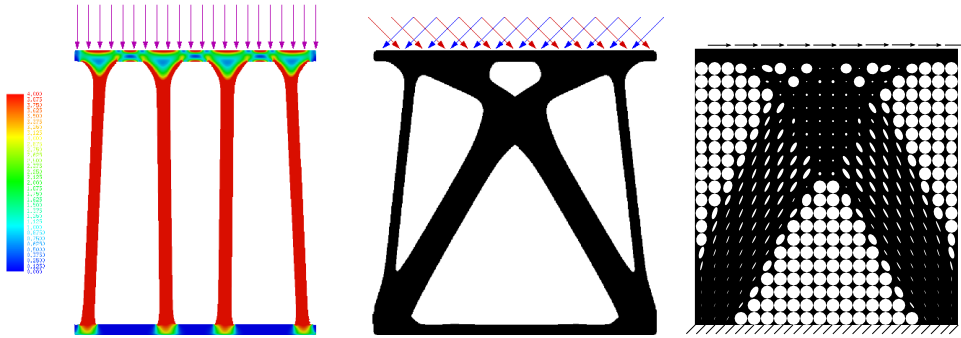

FIGURE 1. A direct comparison of two-stage stochastic optimization and deterministic optimization for an averaged load is shown. In the middle, a stochastically optimal shape is rendered together with the two underlying load scenarios ω_1 and ω_2 on the upper plate, with surface loads $g(\omega_1)$ and $g(\omega_2)$ both with probability $\frac{1}{2}$. On the left the optimal shape colorcoded with the von Mises stress is drawn for a deterministic load $\frac{1}{2}g(\omega_1) + \frac{1}{2}g(\omega_2)$. An optimal shape for a perforated domain under deterministic shear load is shown on the right. (left and center panel reprinted from [25, Fig. 4.2])

4. Stochastic Shape Optimization Models

Two-Stage Stochastic Programming in Finite Dimension. Finite-dimensional linear stochastic programs serve as blueprints for our stochastic shape optimization models. For a quick review consider the initial random optimization problem

$$\min\{c^\top x + q^\top y \ : \ Tx + Wy = z(\omega), \ \ x \in X, \ y \in Y\}, \tag{10}$$

for polyhedra X, Y in Euclidean spaces, together with the information constraint

$$\text{decide } x \mapsto \ \text{observe } z(\omega) \mapsto \ \text{decide } y = y(x, z(\omega)). \tag{11}$$

Hence, problem (10) is accompanied by a two-stage scheme of alternating decision and observation, where the first-stage decision x must not anticipate future information on the random data $z(\omega)$. The second-stage decision $y = y(x, z(\omega))$ often is interpreted as a recourse action. It is taken as an optimal solution to the second-stage problem, *i. e.*, the minimization problem remaining after x and $z(\omega)$ were fixed. The overall aim is to find an x which is "optimal" under these circumstances. Assume the minimum in (10) exists and rewrite

$$\begin{aligned}
&\min_x \left\{c^\top x + \min_y \{q^\top y \ : \ Wy = z(\omega) - Tx, \ y \in Y\} \ : \ x \in X\right\} \\
=\ &\min\{c^\top x + \Phi(z(\omega) - Tx) \ : \ x \in X\} \\
=\ &\min\{\mathrm{j}(x, \omega) \ : \ x \in X\}
\end{aligned} \tag{12}$$

where $\Phi(v) := \min\{q^\top y \ : \ Wy = v, y \in Y\}$ is the value function of a linear program with parameters in the right-hand side.

The representation (12) now gives rise to understanding the search for an "optimal" x as the search for a "minimal" member in the family of random variables $\{\mathrm{j}(x, \omega) \ : \ x \in X\}$. Different modes of ranking random variables then lead to different types of stochastic programs. In a risk neutral setting the ranking is done by taking the expectation $\mathbb{E}_\omega$, leading to

$$\min\{Q_{\mathrm{EV}}(x) := \mathbb{E}_\omega(\mathrm{j}(x, \omega)) \ : \ x \in X\}$$

which is a well-defined optimization problem under mild conditions. With risk aversion, the expectation is replaced by statistical parameters reflecting some perception of risk (risk measures). As examples let us mention minimization of the expected excess of some preselected target $\eta \in \mathbb{R}$

$$\min\{Q_{EE_\eta}(x) := \mathbb{E}_\omega(\max\{\mathrm{j}(x, \omega) - \eta, 0\}) \ : \ x \in X\},$$

and minimization of the excess probability of some preselected $\eta \in \mathbb{R}$

$$\min\{Q_{EP_\eta}(x) := \mathbb{P}_\omega(\mathrm{j}(x, \omega) > \eta) \ : \ x \in X\}.$$

Beside these pure expectation and risk models there are mean-risk models where weighted sums of expected value and risk expressions are minimized, for further details see [47, 51, 56].

Two-Stage Stochastic Programming Formulation of Shape Optimization. In the optimization problem (6) there is a natural information constraint stating that first, and independently of the realizations of the forces $f(\omega), g(\omega)$, the shape $\mathcal{O}$ has to be selected. Then, after observation of $f(\omega), g(\omega)$, (1) determines the displacement field $u = u(\mathcal{O}, \omega)$, leading to the objective value $J(\mathcal{O}, \omega)$. This manifests the interpretation of (6) as a two-stage random optimization problem: In the outer optimization, or first stage, the nonanticipative decision on $\mathcal{O}$ has to be taken. After observation of $f(\omega), g(\omega)$ the second-stage optimization problem is the variational problem of linearized elasticity, where for a fixed elastic domain $\mathcal{O}$ and random state ω one seeks a displacement u minimizing the energy $E(\mathcal{O}, u, \omega)$ defined in (2).

This second-stage optimization process is neither associated with further stochastic parameters nor with the optimization of additional material properties. In fact, it consists of the determination of the elastic displacement, which in turn is required for the computation of the elastic energy and the cost functional. Even though there is no additional decision making involved, the variational structure of the elasticity problem we are solving gives an obvious analogy to the second-stage problem in finite-dimensional stochastic programming.

As counterpart to (11), the information constraint

$$\text{decide } \mathcal{O} \mapsto \ \text{observe } \omega \mapsto \ \text{compute } u = u(\mathcal{O}, \omega).$$

must be fulfilled. The role of $j(x, \omega)$ in (12) then is taken by $J(\mathcal{O}, \omega)$ from (5). Altogether, the random shape optimization problem (6)

$$\min\{J(\mathcal{O}, \omega) : \mathcal{O} \in \mathcal{U}_{\mathrm{ad}}\}$$

arises as the analogon to (12). It amounts to finding a "minimal" member in the family of random variables

$$\{J(\mathcal{O}, \omega) : \mathcal{O} \in \mathcal{U}_{\mathrm{ad}}\}.$$

As in the finite-dimensional case, now different ranking modes for random variables give rise to risk neutral and risk averse stochastic shape optimization models. Taking the expectation yields the risk neutral problem

$$\min\{\mathbf{Q}_{\mathrm{EV}}(\mathcal{O}) := \mathbb{E}_\omega(J(\mathcal{O}, \omega)) : \mathcal{O} \in \mathcal{U}_{\mathrm{ad}}\}. \tag{13}$$

Of the variety of risk averse problems arising with the expectation replaced by some risk measure, we study in more detail those given by the expected excess over some preselected target $\eta \in \mathbb{R}$

$$\min\{\mathbf{Q}_{\mathrm{EE}_\eta}(\mathcal{O}) := \mathbb{E}_\omega(\max\{J(\mathcal{O}, \omega) - \eta, 0\}) : \mathcal{O} \in \mathcal{U}_{\mathrm{ad}}\}, \tag{14}$$

and by the excess probability over $\eta \in \mathbb{R}$

$$\min\{\mathbf{Q}_{\mathrm{EP}_\eta}(\mathcal{O}) := \mathbb{P}_\omega(J(\mathcal{O}, \omega) > \eta) : \mathcal{O} \in \mathcal{U}_{\mathrm{ad}}\}. \tag{15}$$

In our applications we use smooth approximations of the max-function in (14) and of the discontinuity caused by the probability in (15). For the expected excess this leads to

$$\mathbf{Q}_{\mathrm{EE}_\eta}^\epsilon(\mathcal{O}) = \mathbb{E}_\omega(q^\epsilon(J(\mathcal{O}, \omega))),$$

where $q^\epsilon(t) := \frac{1}{2}\left(\sqrt{(t-\eta)^2 + \epsilon} + (t - \eta)\right)$, $\epsilon > 0$. For the excess probability we obtain

$$\mathbf{Q}_{\mathrm{EP}_\eta}^\epsilon(\mathcal{O}) = \mathbb{E}_\omega(H^\epsilon(J(\mathcal{O}, \omega)))$$

with $H^\epsilon(t) := \left(1 + e^{-\frac{2(t-\eta)}{\epsilon}}\right)^{-1}$, $\epsilon > 0$. If the random variable ω follows a discrete distribution with scenarios ω_i and probabilities $\pi_i, i = 1, \ldots, N_s$ for an in general large number N_s or scenarios, then

$$\mathbf{Q}_{\mathrm{EV}}(\mathcal{O}) = \sum_{i=1}^{N_s} \pi_i J(\mathcal{O}, \omega_i), \tag{16}$$

and accordingly for $\mathbf{Q}_{\mathrm{EE}_\eta}^\epsilon(\mathcal{O})$ and $\mathbf{Q}_{\mathrm{EP}_\eta}^\epsilon(\mathcal{O})$.

5. Shape Derivatives

Shape derivatives - deterministic case. To compute the shape derivative, we consider variations $\mathcal{O}_v = (\mathrm{Id} + v)(\mathcal{O})$ of a smooth elastic domain $\mathcal{O}$ for a smooth vector field v defined on the working domain D. For the deterministic objective functional

$$\mathbf{J}(\mathcal{O}) := J(\mathcal{O}, u(\mathcal{O})) = \int_\mathcal{O} j(u(\mathcal{O}))\,\mathrm{d}x + \int_{\Gamma_N} k(u(\mathcal{O}))\,\mathrm{d}\mathcal{H}^{d-1}. \tag{17}$$

the shape derivative [27] in the direction v initially takes the form $\mathbf{J}'(\mathcal{O})(v) = J_{,\mathcal{O}}(\mathcal{O}, u(\mathcal{O}))(v) + J_{,u}(\mathcal{O}, u(\mathcal{O}))(u'(\mathcal{O})(v))$. To avoid an evaluation of $u'(\mathcal{O})(v)$ for any test vector field v, one introduces the dual or adjoint problem. In fact, the dual solution $p = p(\mathcal{O}) \in H^1_{\Gamma_D}(\mathcal{O}; \mathbb{R}^d)$ is defined as the minimizer of the dual functional

$$E_{dual}(\mathcal{O}, p) := \frac{1}{2}a(\mathcal{O}, p, p) + l_{dual}(\mathcal{O}, p),$$

with $l_{dual}(\mathcal{O}, p) = \int_\mathcal{O} j'(u)p\,\mathrm{d}x + \int_{\Gamma_N} k'(u)p\,\mathrm{d}\mathcal{H}^{d-1}$. For the (deterministic version of the) compliance objective (7) we observe that $p = -u$. Given p for fixed u and $\mathcal{O}$ we can evaluate the shape derivative of the deterministic cost functional as follows:

$$\begin{aligned}\mathbf{J}'(\mathcal{O})(v) &= J_{,\mathcal{O}}(\mathcal{O}, u(\mathcal{O}))(v) - l_{,\mathcal{O}}(\mathcal{O}, p(\mathcal{O}))(v) + a_{,\mathcal{O}}(\mathcal{O}, u(\mathcal{O}), p(\mathcal{O}))(v) \\ &= \int_{\partial\mathcal{O}} (v \cdot n)\big[j(u(\mathcal{O})) - f\,p(\mathcal{O}) + \mathbf{C}_{ijkl}e_{ij}(u(\mathcal{O}))e_{kl}(p(\mathcal{O}))\big]\mathrm{d}\mathcal{H}^{d-1}.\end{aligned} \tag{18}$$

Let us remark that in a general situation the shape calculus is more subtle. For a discussion of the appropriate differentiation of boundary integrals we refer to [27, 62]. Here, we confine ourselves, as in [25, 24], to the simpler case that homogeneous Neumann boundary conditions are assumed on the part of the boundary which is optimized. Furthermore, let us emphasize that the above classical shape derivative is only admissible in case of additional regularity for the primal solution u and the dual solution p, which holds under sufficiently strong regularity assumptions on loads and geometry of the considered shapes.

Shape derivatives of expectation and risk measures. With a discrete probability distribution as in (16) we compute the shape derivative of the expectation as

$$\mathbf{Q}'_{\mathrm{EV}}(\mathcal{O})(v) = \sum_{i=1}^{N_s} \pi_i\, J'\,(\mathcal{O}, \omega_i)\,(v)\ . \tag{19}$$

For the approximated expected excess and excess probability the chain rule yields

$$\left(\mathbf{Q}^{\epsilon}_{\mathrm{EE}_\eta}\right)'(\mathcal{O})(v) = \sum_{i=1}^{N_s} \frac{\pi_i}{2} J'(\mathcal{O}, \omega_i)(v) \left(\frac{J\,(\mathcal{O}, \omega_i) - \eta}{\sqrt{(J\,(\mathcal{O}, \omega_i) - \eta)^2 + \epsilon}} + 1 \right),$$

$$\left(\mathbf{Q}^{\epsilon}_{\mathrm{EP}_\eta}\right)'(\mathcal{O})(v) = \sum_{i=1}^{N_s} \frac{2}{\epsilon} \pi_i J'(\mathcal{O}, \omega_i)(v)\, e^{-\frac{2}{\epsilon}(J(\mathcal{O}, \omega_i) - \eta)} \left(1 + e^{-\frac{2}{\epsilon}(J(\mathcal{O}, \omega_i) - \eta)}\right)^{-2}.$$

Efficient evaluation primal and dual solutions for realizations of the randomness. So far, it seems that for every realization one has to compute a primal solution $u(\mathcal{O}, \omega_i)$ and a dual solution $p(\mathcal{O}, \omega_i)$. Under our assumption that $j(\cdot)$ and $k(\cdot)$ are linear or quadratic functions, there is a significant algorithm shortcut at our disposal for $N_s \gg 1$, which we will recall here. For details we refer to [25]. Let us assume that there is a small number of (deterministic) basis volume forces $f_1, \ldots, f_{K_1}$, and of (deterministic) basis surface loads $g_1, \ldots, g_{K_2}$. Then, the actual loads $f(\omega)$ and $g(\omega)$, respectively, are given as linear combinations of these deterministic basis loads $f(\omega) = \sum_{i=1}^{K_1} c_i^f(\omega) f_i$ and $g(\omega) = \sum_{j=1}^{K_2} c_j^g(\omega) g_j$, with the uncertain coefficients $c_i^f(\omega) \in \mathbb{R}$, $i = 1, \ldots, K_1$, and $c_j^g(\omega) \in \mathbb{R}$, $j = 1, \ldots, K_2$. The advantage of this approach is that we only need to solve as many elasticity PDEs as there are scenarios in order to evaluate the objective functional for a given shape $\mathcal{O}$. This will reduce the computing cost significantly in case $N_s \gg K_1 + K_2$. Suppose $u^{(i,0)}$ is the elastic displacement for given volume force $f := f_i$ and surface load $g := 0$, for all $i = 1, \ldots, K_1$. Similarly, let $u^{(0,j)}$ be the displacement corresponding to the volume force $f := 0$ and the surface load $g := g_j$, for all $j = 1, \ldots, K_2$. Then,

$$\bar{u}\,(\mathcal{O}; \omega) := \sum_{i=1}^{K_1} c_i^f(\omega) u^{(i,0)} + \sum_{j=1}^{K_2} c_j^g(\omega) u^{(0,j)} \tag{20}$$

is the minimizer of (2) with volume force $f := f(\omega)$, and surface load $g := g(\omega)$. A similar relation holds for the adjoint state $\bar{p}\,(\mathcal{O}; \omega)$ in scenario ω, if we additionally assume that $\sum_{i=1}^{K_1} c_i^f(\omega) + \sum_{j=1}^{K_2} c_j^g(\omega) = 1$, which can always be achieved by choosing the basis forces appropriately. In that case, and if we denote the adjoint states for the individual basis forces by $p^{(i,0)}$ and $p^{(0,j)}$, one obtains

$$\bar{p}\,(\mathcal{O}; \omega) := \sum_{i=1}^{K_1} c_i^f(\omega) p^{(i,0)} + \sum_{j=1}^{K_2} c_j^g(\omega) p^{(0,j)} \tag{21}$$

is the adjoint state belonging to the state $\bar{u}\,(\mathcal{O}; \omega)$.

6. Description of two different classes of admissible shapes

In this section, we will investigate two different shape representations and discuss how to evaluate cost functionals and derivatives with respect to a modification of the shape. On the one hand we will employ a level set method to flexibly describe shapes given as implicit surfaces. On the other hand, geometric details describing an elastic domains will be described by polygonal models determined by a small number of parameters each.

Implicit shapes described via level sets. In many shape optimization problems the topology of the optimal shape is not given a priori. One approach to allow the topology to adapt during a relaxation of the cost functional is to formulate the optimization problem in terms of shapes described by level sets – let us in particular refer to the approach by Allaire and coworkers [3, 4, 5, 8] and to [28, 38, 55]. Explicitly, we assume the elastic body $\mathcal{O}$ to be represented by a level set function ϕ, that is $\mathcal{O} = \{\phi < 0\} := \{x \in D \mid \phi(x) < 0\}$. The boundary $\partial\mathcal{O}$ corresponds to the zero level set of ϕ, i. e., $D \cap \partial\mathcal{O} = \{\phi = 0\}$. Level set methods have originally been used in the context of interface propagation, starting with the pioneering work of Osher and Sethian [43]. Since then the scope of applications was successively widened due to their enormous flexibility. For a general overview we refer to [42, 54]. The core observation in the context of evolving geometries is that for a domain boundary $\partial\mathcal{O}$ propagating with speed v, the corresponding evolution of the level set function ϕ is given by the level set equation $\partial_t \phi + |\nabla\phi| \, v \cdot n = 0$, where $n = \frac{\nabla\phi}{|\nabla\phi|}$ is the field of outer normals on the level sets. In the context of variational problems for shapes, this can be rephrased as follows. The level set equation identifies a variation $s = \partial\phi$ of the level set function with (normal) variations $v \cdot n$ of the level set surfaces. Here, let us refer to Sokolowski and Zolésio [62], who phrased shape sensitive analysis elegantly in terms of level sets. Using this insight, one can rewrite the objective functional $J(\mathcal{O})$ in terms of a level set function ϕ defining $\mathcal{J}(\phi) := J(\{\phi < 0\})$ and then obtain for the shape derivative of the objective functional $\mathcal{J}(\phi)$ with respect to a variation s of ϕ

$$\mathcal{J}'(\phi)(s) = J'(\{\phi < 0\})\left(-s\,|\nabla\phi|^{-1}n\right). \tag{22}$$

This representation of the shape derivative can then be used in a relaxation scheme for the objective functional at first in the deterministic set up. But a generalization to stochastic shape optimization in case of finitely many scenarios is straightforward. We emphasize that the usual level set approach allows only simplifications of the topology during a descent scheme for the cost functionals. New holes can not be created.

Perforated domains with parametrized geometric details. At variance with the usual description of shapes as volumetric macroscopic objects with a piecewise smooth boundary let us now consider a fixed domain D perforated with a large number of holes. In fact, we do not aim to optimize the outer boundary of D but the geometry of the holes inside the domain. Thereby, we perform an optimization of the fine-scale geometric structure of the elastic object. In the application section, we will comment on the relation of this type of shape optimization to homogenization approaches in shape optimization. As a structural restriction let us assume that the fine scale geometric details are centered at the nodes of a lattice covering the domain D. The considered fine scale geometry is parametrized over a low dimensional set of parameters. Furthermore, we restrict ourselves here to N elliptical holes $\mathcal{B}(c_i, \alpha_i, a_i, b_i)$ $(1 \leq i \leq N)$, parametrized by a rotation α_i and two scaling factors a_i and b_i for the two semi-axes, i. e.

$$x(s) = c_i + h \left(\begin{array}{c} a_i \cos(\alpha_i)\cos(s) - b_i \sin(\alpha_i)\sin(s) \\ a_i \sin(\alpha_i)\cos(s) + b_i \cos(\alpha_i)\sin(s) \end{array} \right)$$

where h is the grid size of the lattice and the center points are characterized by $\frac{c_i}{h} + \frac{1}{2} \in \mathbb{Z}$. To avoid overlapping of adjacent or completely vanishing holes we require the scaling parameters to be bounded, i. e. we require $\epsilon \leq a_i, b_i \leq \frac{1}{2} - \epsilon$ with $\epsilon > 0$ being a small additional offset to prevent numerical instability. Finally, we impose a constraint on the total 2D volume of elastic object $\mathcal{O} := D \setminus (\bigcup_{i=1,\ldots,N} \mathcal{B}(c_i, \alpha_i, a_i, b_i))$ and require $|D| - \sum_{i=1}^{N} \pi h^2 a_i b_i = V$. If we assume that ellipses are attached to a fixed set of cell center c_i in D, then the resulting shape optimization problem turns into a finite dimensional optimization problem in $\mathbb{R}^{3N}$ with inequality constraint for the a_i and b_i and one equality constraint due to the prescribed total 2D volume. The associated cost function is given by

$$\mathcal{J}((\alpha_i, a_i, b_i)_{i=1,\ldots,N}) := J\left(D \setminus \left(\bigcup_{i=1,\ldots,N} \mathcal{B}(c_i, \alpha_i, a_i, b_i)\right)\right),$$

for which one easily derives the shape gradient

$$\mathcal{J}'((\alpha_i, a_i, b_i)_{i=1,\ldots,N}) = \left((\partial_{\alpha_j}\mathcal{J}, \partial_{a_j}\mathcal{J}, \partial_{b_j}\mathcal{J})((\alpha_i, a_i, b_i)_{i=1,\ldots,N})\right)_{j=1,\ldots,N}$$

as a vector in $\mathbb{R}^{3N}$. In this context, we are in particular interested in the interaction of different holes with respect to the shape optimization.

7. A sketch of the numerical algorithms

In this section we detail the numerical algorithms in two space dimensions ($d = 2$). On the one hand we discuss a finite element approach for the level-set-based shape optimization and in particular describe suitable finite element spaces for the primal and the dual solutions. Furthermore, we discuss how to combine the topological derivative and the regularized gradient descent approaches in a robust discrete-energy minimization. On the other hand we review the boundary element method as a tool to calculate the cost functional and its gradient in case of perforated domains with fine scale geometries.

Finite element discretization of the level set approach. For the ease of implementation we restrict ourselves to the working domain $D = [0, 1]^2$. We suppose that a dyadic hierarchy of regular grids is given and each cell is supposed to be divided along one of the diagonals into two triangles. Let $\mathcal{V}_h$ be the corresponding space of piecewise affine functions on the resulting triangular grid, where $h = 2^{-l}$ on level l of the grid hierarchy. A discrete level set function $\Phi \in \mathcal{V}_h$ identifies a discrete, polygonally bounded elastic body $\mathcal{O}_h = \{x \in D : \Phi(x) < 0\}$. To avoid either inaccurate evaluations of the objective functional and the shape derivative or a complicated regular remeshing of the boundary $\partial \mathcal{O}_h$ [29, 44] we resort to composite finite elements. Introduced by Hackbusch and Sauter [34] they allow for efficient multigrid solvers for elliptic problems on complicated domains. In fact, we define vector-valued composite finite element basis function $\Theta_{ij}^{\mathrm{cfe}}(x) = e_j \, \chi_{\mathcal{O}_h}(x) \, \Theta_i(x)$, where Θ_i is one of the usual nodal basis functions of $\mathcal{V}_h$ and $e_1 = (1, 0)$, $e_2 = (0, 1)$. Here, $\chi_{\mathcal{O}_h}$ denotes the characteristic function of $\mathcal{O}_h$. Collecting all of these tailored basis functions which vanish on the Dirichlet boundary Γ_D we span the composite finite element space $\mathcal{V}_h^{\mathrm{cfe}}$. Notice that to keep the Dirichlet boundary and the inhomogeneous Neumann boundary fixed we freeze the level set function Φ on a small neighborhood of $\Gamma_D \cup \Gamma_N$ (cf. the problem set up in Section 3). Hence, in this region the body still behaves elastically, but does not undergo any optimization. For a given basis load the discrete primal solution is defined as the finite element function $U^{i,j} \in \mathcal{V}_h^{\mathrm{cfe}}$ solving $A(\mathcal{O}_h, U^{i,j}, \Theta) = l^{i,j}(\mathcal{O}_h, \Theta)$ for all $\Theta \in \mathcal{V}_h^{\mathrm{cfe}}$, where $l^{i,0}(\mathcal{O}_h, \Theta) := \int_{\mathcal{O}_h} f_i \cdot \Theta \, \mathrm{d}x$ and $l^{0,j}(\mathcal{O}_h, \Theta) := \int_{\partial \mathcal{O}_h} g_j \cdot \Theta \, \mathrm{d}\mathcal{H}^{d-1}$ for $1 \le i \le K_1$ and $1 \le j \le K_2$. The corresponding set of dual solutions are those functions $P^{i,j} \in \mathcal{V}_h^{\mathrm{cfe}}$, for which $A(\mathcal{O}_h, \Theta, P^{i,j}) = -J_{,u}(\mathcal{O}_h, U^{i,j})(\Theta)$. for all $\Theta \in \mathcal{V}_h^{\mathrm{cfe}}$. Due to the assumption on $J(\mathcal{O}, \cdot)$ the integrand is at most quadratic and can be integrated exactly using a Gauss quadrature rule. Finally, the primal and dual solutions for the actual set of realizations ω_i for $i = 1, \ldots, N_S$ are composed of the discrete primal and dual solutions $U^{i,j}$ and $P^{i,j}$, respectively, based on the discrete analog of (20) and (21), respectively. For further details on the primal and dual solutions we refer to [25] and for the composite finite element approach in the context of domains described via level sets we refer to [37].

For the relaxation of the shape functional we consider a time discrete, regularized gradient descent for the risk measure $\mathbf{Q}$ defined on shapes now described by level set functions (in case of the basic expected value model $\mathcal{Q}(\Phi) := \mathbb{E}\left(\mathcal{J}(\Phi, \omega)\right)$). Explicitly, given an level set function Φ^k we compute Φ^{k+1} in the next iteration solving

$$\mathcal{G}(\Phi^{k+1} - \Phi^k, \Psi) = -\tau \mathbf{Q}'(\Phi^k)(\Psi) \tag{23}$$

for all $\Phi \in \mathcal{V}^h$. Here $\mathcal{G}$ is the following H^1-type metric on the space of variations of the level set function ϕ (cf. [45])

$$\mathcal{G}(\zeta, \xi) = \int_D \zeta \xi + \frac{\rho^2}{2} \nabla \zeta \cdot \nabla \xi \, \mathrm{d}x, \tag{24}$$

which is related to a Gaussian filtering of the L^2 gradient with the filter width ρ. Furthermore, we consider Armijo rule as a step size control. For an overview on optimal design based on level sets and suitable energy descent methods we refer to a recent survey by Burger and Osher [18]. Finally, after a fixed number of gradient descent steps we use a thresholding with respect to the topological derivative to enable the creation of new holes in the elastic domain. This relaxation algorithm is now applied in a coarse to fine manner. Starting on coarse grids, we successively solve the minimization and prolongate on the next finer grid level until the a priori given finest grid resolution is reached. A regularization corresponding to a surface area term is implemented via a morphological operator as discussed in [25].
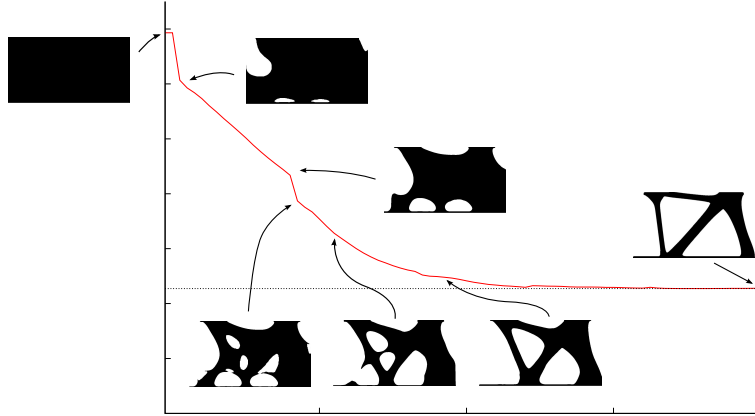
FIGURE 2. The energy decay is depicted and some intermediate time steps are shown for the successive shape relaxation via the level set / CFE method. The impact of the topological derivative can be seen two times, first directly at the start of the algorithm and second associated with a jump of the energy during the relaxation process.

Boundary element approach in the context of perforated domains. We will now briefly review the Boundary Element Method which is used to solve the primal and dual problem in the context of perforated domains. Main ingredient is a fundamental solution for the PDE of linearized elasticity [23]. Identifying points $x \in \mathbb{R}^2$ with points $z(x) = x_1 + p\, x_2$ on the complex plane, where p is a complex constant, which is used in order to transform balls into ellipses, the fundamental solution u_{ki}^* and its normal derivative v_{ki}^* are given by

$$u_{ki}^* = \frac{1}{2\pi} \sum_m \Re\left\{ \sum_n A_{kn} N_{nj} \, \ln\left(z_n(x-y)\right) \right\} d_{mi}\,, \quad v_{ki}^* = -\frac{1}{2\pi} \sum_{j,m} \Re\left\{ \sum_n \frac{D_{ijn} N_{nm}}{z_n(x-y)} \right\} d_{mi}\, n_j\,.$$

Here n denotes the outer normal and A_{kn}, N_{nj}, D_{ijn}, d_{mi} are appropriately chosen constants. We now consider equation (2), apply Green's formula, substitute ϑ by the fundamental solutions u_i^* and arrive at

$$u_{ki}(x) = \int_{\partial\mathcal{O}} (\mathbf{C}\varepsilon(u)n) \cdot u_{ki}^* \, d\mathcal{H}^1(y) - \int_{\partial\mathcal{O}} (\mathbf{C}\varepsilon(u_{ki}^*)n) \cdot u \, d\mathcal{H}^1(y) + \int_{\mathcal{O}} f \cdot u_{ki}^* \, dy. \qquad (25)$$

From this formula one now derives in the usual way a collocation type boundary element method (for details we refer to [33]). Under the assumption that $f \equiv 0$, for u on the boundary and $\sigma_n = \mathbf{C}\varepsilon(u)n$ denoting the normal tensions at the boundary we obtain from (25) the integral equation

$$u = U[\sigma_n] - V[u]\,, \qquad (26)$$

where $U[\sigma_n]$ is a *single layer operator* and $V[u]$ a *double layer operator* .

For the discretization we restrict ourselves to polygonal domains $\mathcal{O}_h$, where the ellipses and the outer boundary are replaced by polygons with a fixed number of vertices, which are considered as *collocation points*. Effectively, these points depend on the free parameters c_i, α_i, a_i, and b_i of the ellipses. Furthermore, we approximate u and σ_n on the boundary via piecewise affine, continuous functions. Equation (26) must now hold for every collocation point leading to a linear system of equations for the values of the displacement and the normal tensions at each point. To evaluate the objective funtionals observe that (7) and (9) have already been phrased as boundary integrals. Shape derivatives of the objectives are also expressed in terms of boundary integrals in (18). For the evaluation of these integrals full gradients of the primal and dual solution are required whereas we only have (discrete approximations) of the normal stresses at our disposal so far. However

one can reconstruct them approximately using finite differences on the polygonal boundary for the tangential derivatives of the displacement. Thus, we are able to write suitable approximations of the objective functional and the shape derivative in terms of the vector of free parameters $(\alpha_i, a_i, b_i)_{i=1,\dots,N}$. The treatment of the resulting finite dimensional constrained optimization problems is a classical and well developed field. For our problem we rely on the software package `Ipopt` [64, 65] which implements a Primal-Dual Interior Point Filter Line Search algorithm. Fig. 7 shows a plot of energy during optimization by `Ipopt` together with some intermediate results.
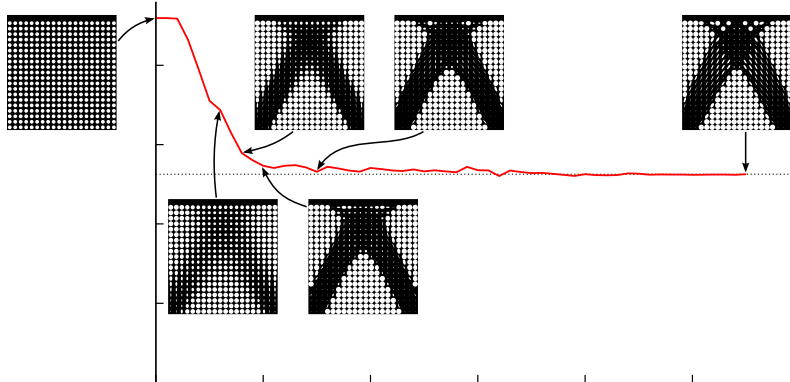
FIGURE 3. The energy during optimization of a perforated square domain under shear load by `Ipopt` is plotted with the final value indicated by the dashed line.

8. Applications of stochastic risk measure optimization

In this section we present several applications of the methods discussed before. We discuss the stochastic optimization in the context of shapes described by level sets and by parametrized geometry (and also shortly compare the latter with results derived by the homogenization method). Furthermore, we give a detailed description of the results obtained by using risk averse stochastic optimization.

Stochastic Optimization of a 2D carrier plate. As a first application we look at a 2D carrier plate, where the supporting construction between a floor slap, whose lower boundary is assumed to be the Dirichlet boundary, and an upper plate, on which forces act, is optimized. The working domain is $D = [0,1]^2$.

Figure 1 (left and center) shows a straightforward comparison between a stochastic optimization as described before and an optimization for a deterministic load corresponding to the expected value of the stochastic loads. Also the corresponding optimal shape (for a deterministic load) with fine scale parametrized geometry is shown on the right. For comparison Fig. 4 depicts additional results in the context of perforated domains under similar loading conditions colorcoded by the von Mises stress. One observes a rather sharp interface between regions with high and low volume fraction of the elliptical holes. Furthermore, the resulting shapes are roughly similar to the ones obtained in the level set context but have additionally developed fine trusses aligned with the main loading directions. For the image generation in Fig. 4 a triangulation of the computational domain was created using the software `Triangle` [57, 58] and at each interior vertex the linearized strain tensor is computed using (25).

Our next case study is a more elaborate example for stochastic optimization in the context of level sets. Fig. 5 shows a sketch of the stochastic loading on the upper plate and the (single) stochastically optimal shape obtained by the level-set based stochastic optimization algorithm. Furthermore, the von Mises stress distribution is rendered for the different load scenarios. Since each realization of the stochastic load is chosen to be spatially uniform on the upper plate, the realizations only differ by the direction of the force. Hence, the load space containing all realizations of the stochastic loads can be represented by the span of two base loads g^1 and g^2. In the notation of Section 5, we have $K_2 = 2$ and $N_S = 20$.
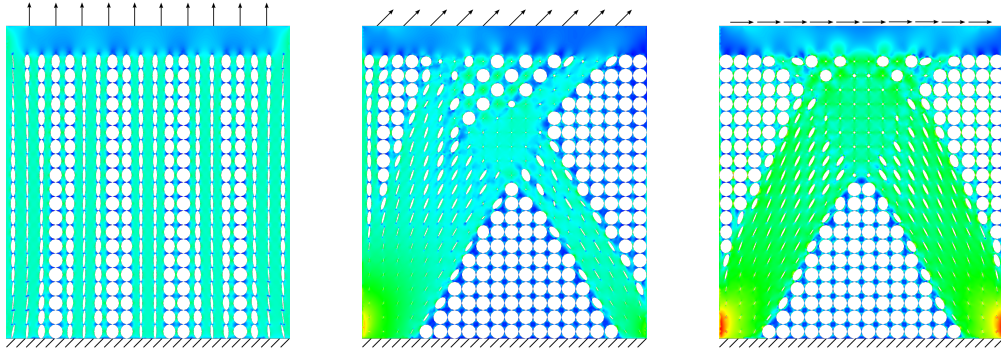
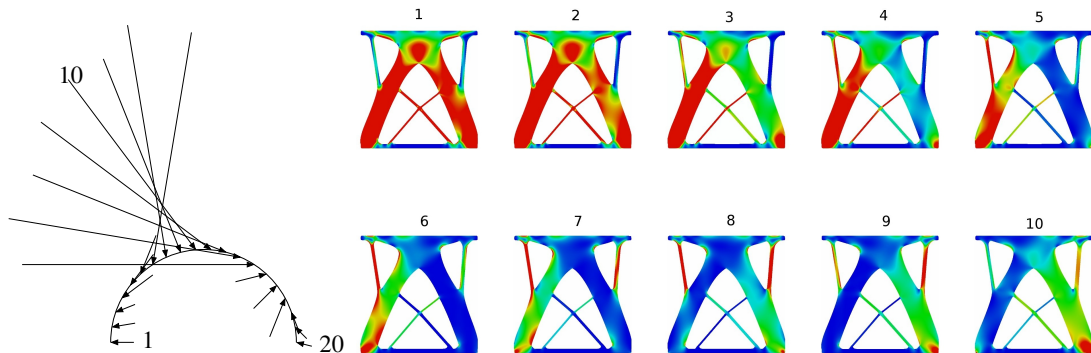FIGURE 4. Different loads and corresponding optimal shapes colorcoded by the von Mises stress.

FIGURE 5. Stochastic shape optimization based on 20 scenarios is depicted. On the left the different loads $g(\omega_\sigma)$ with probabilities π_σ are sketched. Each arrow represents one scenario where the arrow length is determined by the corresponding force intensity weighted with the probability π_σ of the corresponding scenario. On the right the von Mises stress distribution is colorcoded on the optimal shape for 10 out of the 20 realizations of the stochastic loading. Due to the nonsymmetric loading configuration the resulting shape is nonsymmetric as well. In particular, the right carrier is significantly thicker than the left one, whereas the connecting diagonal stray pointing up right is thinner than the one point down left. (Figure reprinted from [25, Fig. 4.3])

2D and 3D cantilever. As a second application, we discuss the shape optimization of a 2D cantilever. We choose $D = [0, 2] \times [0, 1]$ and model a cantilever that is fixed on the left side and where a deterministic downward pointing force is applied on a small plate on the right. Three methods, namely homogenization (by Allaire [3], first with a composite solution and then with a penalization of composite regions), level set based optimization, and optimization of a perforated geometry are used to create the results shown in Fig. 6 (rotated by 90 degrees). Also, for the latter two methods, the von Mises stress is shown by colorcoding.

As a generalization of the application before, we now consider a 3D cantilever. Here again the cantilever is fixed on one side by having a Dirichlet condition on a disk-shaped plate. Whereas on the other side we prescribe a Neumann boundary load on a small rectangular plate opposite to the center of the disk. Applying eight stochastic loading scenarios with equally probable and equally distributed forces in a plane parallel to the disk-shaped plate results in the optimal shape shown in Fig. 7. Again a colorcoding of the von Mises stress distribution is displayed.
2D bridge. For the sake of completeness also a typical bridge-type scenario was investigated in the context of perforated domains. Here the computational domain was chosen as $D = [0, 3] \times [0, 1]$, the lower corners were kept fixed by imposing Dirichlet boundary values and the remainder of the lower boundary was subject to downward pointing forces. Fig. 8 shows the obtained result
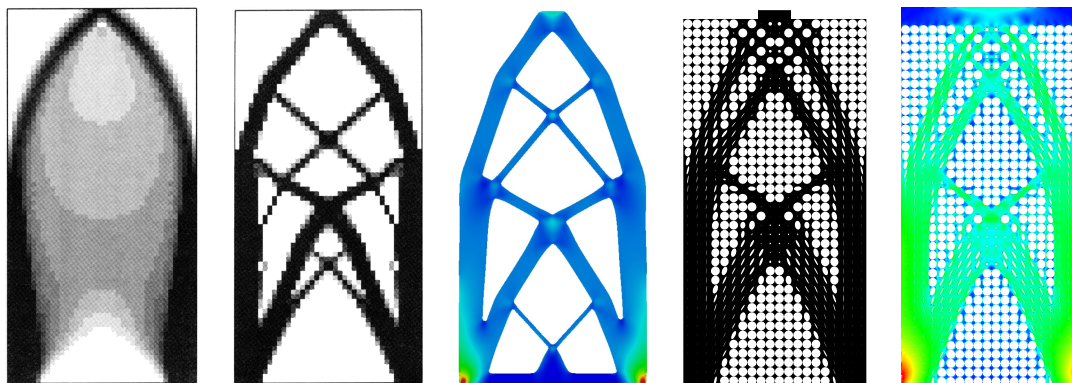
FIGURE 6. Comparison between optimal shapes for the cantilever scenario obtained by the homogenization method by Allaire (first two panels, reprinted from [3, Fig. 5.8, p. 370]), level set based optimization (central panel, reprinted from [25, Fig. 4.5]), and optimization of perforated geometries.
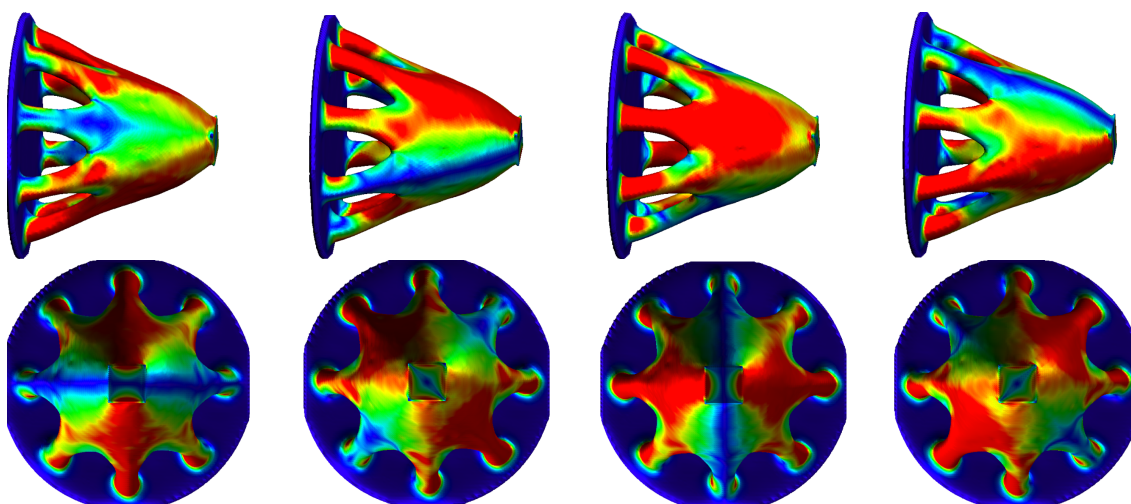

FIGURE 7. The optimal design in the case of stochastic shape optimization for the cantilever problem with eight scenarios is depicted. From left to right four scenarios are colorcoded with the von Mises stress in a consecutive clockwise ordering with respect to the attacking loads. The upper and the lower row show the shape geometry under different perspectives. (Figure reprinted from [25, Fig. 4.8])

colorcoded with the von Mises stress and again in comparison to results of the homogenization method.

Trusses underneath two fixed bearings. In this section we will discuss an application with the focus on risk averse stochastic optimization and study the impact of different risk measures on the optimal shape. First, we discuss the optimization of the expected-value objective. We consider two instances with 10 loading scenarios each (shown in Fig. 9). In the first instance (plotted on the left) all scenarios have the same probabilities and all scenario loads have the same magnitude. In the second instance (plotted on the right) we deal with an asymmetric case: loads acting on the left bearing are twice as strong as those acting on the right bearing. But the left loads have a much lower probability of 0.01 whereas each load on the right is active with probability 0.19. Hence, on average, the forces acting on the left bearing play a minor role. In both instances, the number of base forces is 4 (i.e, $K_2 = 4$), since two of them have their support only at the left bearing, whereas the other two apply only on top of the right bearing. The shapes shown in Fig. 9 minimize the expected value of the compliance cost functional. It can be observed that the symmetric load configuration leads to a symmetric truss construction, whereas for nonsymmetric loading nonsymmetric outriggers
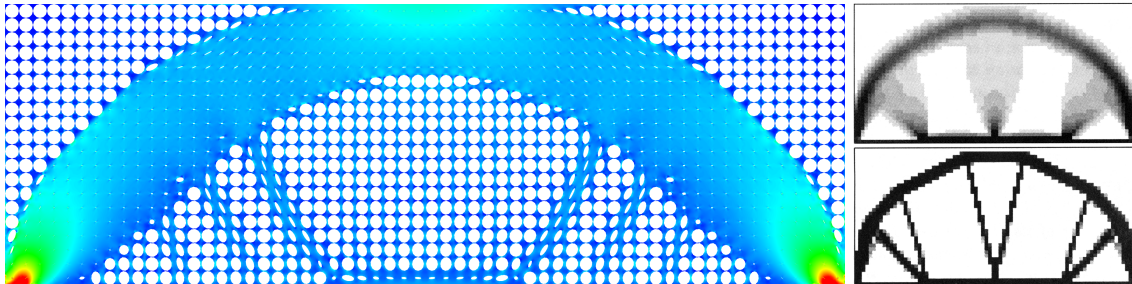
FIGURE 8. Comparison between optimal shapes for the bridge scenario obtained by Allaire with the homogenization method (right panel, reprinted from [3, Fig. 5.28, p. 399]) and optimization of perforated geometries.
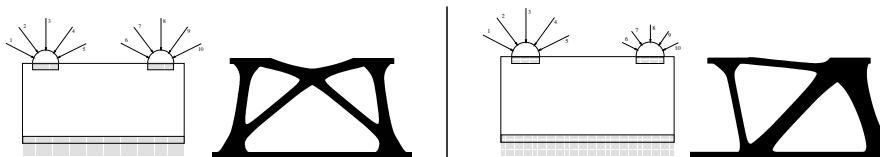

FIGURE 9. A symmetric stochastic load configuration (left) leads to symmetric support jibs (left panel), whereas a nonsymmetric stochastic loading (right panel) favors a correspondingly nonsymmetric truss construction. (Figure reprinted from [24, Fig. 4])
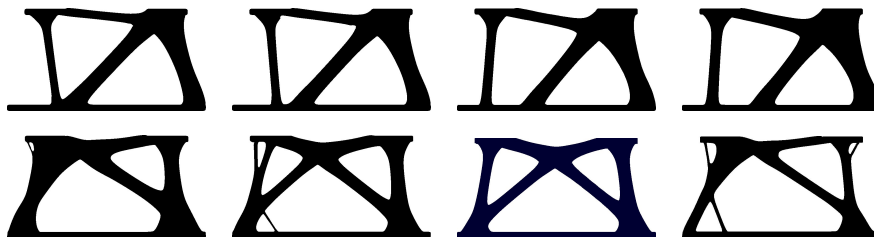

FIGURE 10. A sequence of results for the optimization with respect to the expected excess for $\eta = 0.1, 0.2, 0.3, 0.4, 0.6, 0.8, 1.0, 1.5$. The underlying loading is shown in Fig. 9 (right panel). (Figure reprinted from [24, Fig. 5])

minimize the expected value of the cost. Figure 7 shows the energy decay and selected snapshots of the evolving shape for the level-set based method. The intermediate results illustrate the interplay between hole creation by thresholding based on the topological derivative and the optimization of the boundary by the level set / CFE method.

Expected Excess. As mentioned above, one of the main objectives of this section is to compare the different risk measures and we will discuss this in the context of the second (nonsymmetric) load configuration. Fig. 10 shows a family of optimal shapes minimizing the expected excess for varying excess parameter η. Although we start each computation with the same initial solid bulk domain $\mathcal{O}_0 = D$, we observe a continuous evolution of the geometry with η. Due to the nonanticipativity of our stochastic shape optimization model, the actual loading on an optimal shape, but not the shape itself, depends on the load scenario.

Is is important to point out that in the minimization of the expected excess all the scenarios ω where $J(\mathcal{O}, \omega) \leq \eta$ are irrelevant. In practice, since we use the smooth approximation $\mathbf{Q}_{\mathrm{EE}_\eta}^\epsilon$ (see Section 4) to regularize the stochastic cost functional, these scenarios still have a small effect. Hence, the optimization tries to choose $\mathcal{O}$ such that the objective $J(\mathcal{O}, \omega)$ stays below the risk parameter η in the high-probability, and therefore "expensive" scenarios, which correspond to load acting on the right bearings. In fact, the higher the value of η is, the easier it is to keep the objective below η. This leads to the effect that less material is needed on the right and therefore more

material can be used to improve the situation for the scenarios with the strong but low-probability loading on the left bearing.

An analogous computation was done in the framework of perforated domains. In Fig. 11 one can observe qualitatively the same behaviour as seen in the level-set based computation. In particular, one observes that for high η the initial configuration remains unchanged, since due to the small offset ϵ (cf. section 6) there is no need for improvement to stay below the excess parameter. We have to remark that because of the different scaling of the attacking forces the values of the parameter η in the two computations are not directly comparable.

(a) 0.0003   (b) 0.0005   (c) 0.0007

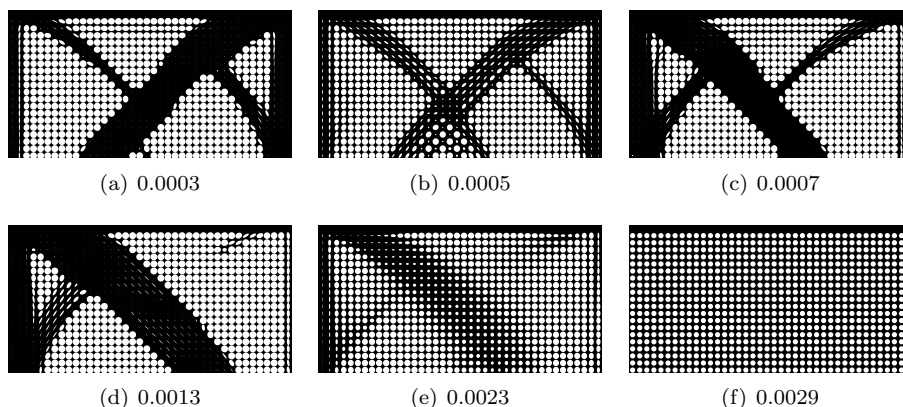(d) 0.0013   (e) 0.0023   (f) 0.0029

FIGURE 11. A sequence of results for the optimization with respect to the expected excess for $\eta = 0.0003, 0.0005, 0.0007, 0.0013, 0.0023, 0.0029$. The underlying loading is shown in Fig. 9 (right panel).

(a) 0.0003   (b) 0.0005   (c) 0.0007
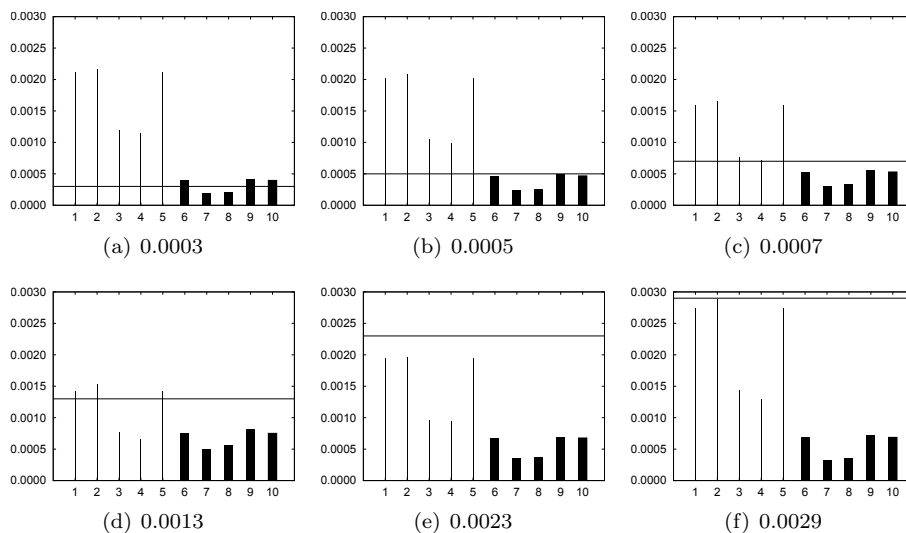
(d) 0.0013   (e) 0.0023   (f) 0.0029

FIGURE 12. Objective values for each of the 10 scenarios are rendered with bar charts for the optimal shapes in Fig. 11. The bar thickness is chosen proportional to the probability.

Excess Probability. We now turn to optimizing the excess probability. Albeit somewhat related, strikingly different shapes are being realized. Looking at Fig. 13 one observes a complete "mass shift" towards the right bearing. The important difference to the expected excess is that the amount of excess is irrelevant here. Therefore huge objective values may be acceptable for the five (low-probability) scenarios on the left as long as it is possible to push the corresponding values for the

(high-probability) scenarios on the right bearing below η (cf. Fig. 15 for the corresponding cost diagram). Consequently trusses for the left bearing are allowed to become thinner as η increases. This can be seen in Fig. 13 but even better for the combined level set and topological shape optimization approach in Fig. 14 where finally the narrow trusses are removed via a topology optimization step.
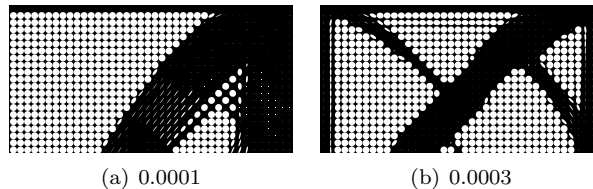

(a) 0.0001   (b) 0.0003

FIGURE 13. Two results for the optimization with respect to the excess probability for $\eta = 0.0001, 0.0003$. The underlying loading is shown in Fig. 9 (second right)

FIGURE 14. In the optimization of the excess probability for $\eta = 0.4$ decreasingly thin trusses are realized on the intermediate grey shape on the left until the left bearing is completely truncated via a topology optimization step (cf. Fig. 9 for the load configuration). The final result is shown on the right. (Figure reprinted from [24, Fig. 7])

Let us conclude with a final review of the three considered risk measures. Fig. 15 shows objective values for each loading scenario at the optimal for the different risk measures. The expected value causes a weighted average over all single-scenario realizations. Therefore objective values for high-probability scenarios are reduced as much as possible whereas rather big values are accepted for the low-probability scenarios. For the expected excess the main difference is that there is no need to further optimize scenarios whose objective values have already been pushed below the threshold. The gained flexibility may instead be used to reduce the cost of scenarios above η more aggressively. Finally the excess probability reduces the process of assigning an objective value to the question of how likely scenarios exceeding the threshold occur. The consequence is ignorance of objective values for scenarios significantly above the threshold, which may be considered to be "lost" anyway. In the figure discussed before, a compliance tending to infinity is indeed accepted when the left bearing is left floating. The arising flexibility is then used to further reduce maximal (weighted) scenarios whose costs are slightly bigger than the threshold. As to the built–in regularization in $\mathbf{Q}^{\epsilon}_{\mathrm{EE}_\eta}, \mathbf{Q}^{\epsilon}_{\mathrm{EP}_\eta}$ one has to remark that the discussed threshold behavior is smeared out at η, thereby favoring cost reduction of single scenarios in the vicinity of the threshold.

9. Hole-hole interaction in the topological derivative

Introducing topological derivatives. As discussed in the Introduction, classical shape-optimization methods are based on iteratively improving a given shape $\mathcal{O}$, by determining at each step an optimal small modification to the position of the boundary $\partial\mathcal{O}$, and are therefore unable to change the topology of the shape. The method of topology optimization is based on a determination of the gradient of the functional with respect to changes in topology of $\mathcal{O}$ [59, 31]. Precisely, for $\bar{x} \in \mathcal{O}$ one considers the family of domains $\mathcal{O} \setminus B(\bar{x}, \rho)$. The topology derivative at x is then defined as the limit $\lim_{\rho \to 0}(J[\mathcal{O} \setminus B(\bar{x}, \rho)] - J[\mathcal{O}])/\rho^n$, where J is the target functional. As usual in PDE-constrained optimization the target functional depends indirectly on $\mathcal{O}$, through a function u which is obtained
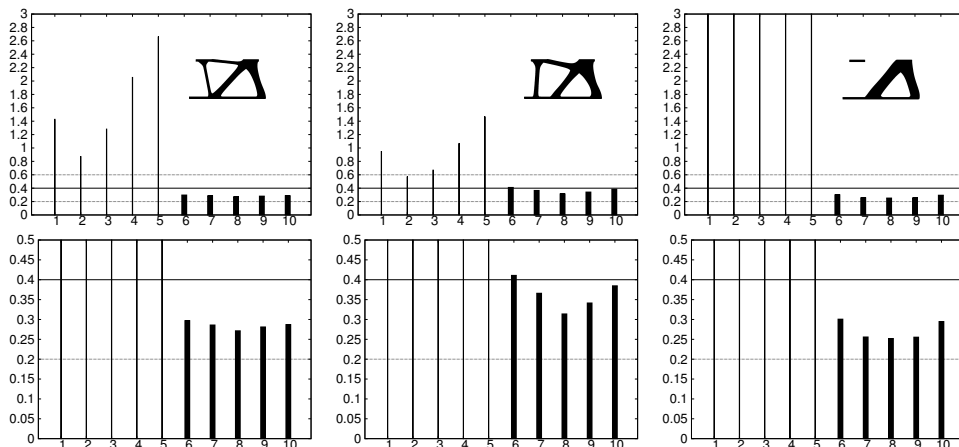
FIGURE 15. Objective values for each of the 10 scenarios are rendered with bar charts for the optimal shapes corresponding to the stochastic cost functionals $\mathbf{Q}_{\mathrm{EV}}$, $\mathbf{Q}_{\mathrm{EE}_\eta}^\epsilon$, $\mathbf{Q}_{\mathrm{EP}_\eta}^\epsilon$ (from left to the right) for $\eta = 0.4$. The second row shows a zoom into the diagrams. The bar thickness is chosen proportional to the probability. (Figure reprinted from [24, Fig. 8])

by solving a PDE, which in our case corresponds to linear elasticity. Therefore an analytic evaluation of the topological derivatives requires a determination of the leading-order correction to the elastic deformation arising from the formation of a small hole [31]. This is done by a separation of length scales, between the one where the hole acts and the macroscopic one of $\mathcal{O}$; the interaction between the two can be represented by a suitable Dirichlet-to-Neumann operator acting on the new (fictitious) boundary. Thus, the inner problem can be analytically solved, depending on the local values of the strain coming from the exterior problem. The topological derivative is then evaluated numerically, and used to modify the computational domain $\mathcal{O}$.

Interaction between holes. As explained above the topological derivative describes the behaviour of the cost functional with respect to the removal of a small hole. In practice, it is often used to remove a complete area, determined as the set where the derivative is below a threshold (see Section 7). This and also the observed hole structures in Section 6 (see Fig. 16(a)) motivate the study of an asymptotic expansion with respect to multiple holes on a lattice as in

$$J\left(\mathcal{O} \setminus \bigcup_{z \in \mathbb{Z}^n} \delta z + \epsilon\omega\right) = J(\mathcal{O}) + \dots \tag{27}$$
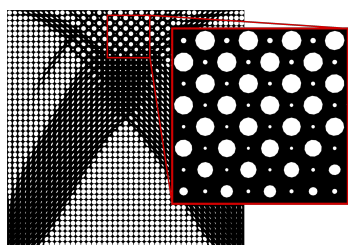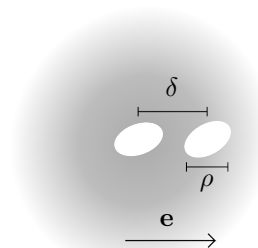
(a)   (b)

FIGURE 16. Fig. (a) shows some hole structures observed in the optimization of parametrized domains (see Section 6) and Fig. (b) gives a small sketch of the two-hole problem dealt with in Theorem 1

We start by studying the interaction between two holes (see Fig. 16(b) for a sketch). In order to make the notation easier we deal with the scalar case, by considering the Poisson equation on

the set $\mathcal{O}$ (note that one can also apply an analogous result to the case of linear elasticity). Here $a_0(u, v)$ is the corresponding bilinear form and u_0 the solution to the equation. Let $\omega_1, \omega_2 \subset \mathbb{R}^2$ be the shapes of the two holes and for convenience assume that both contain the origin. We also define the sets $\mathcal{O}_R = \mathcal{O} \setminus B(\bar{x}, R)$, the new fictitious boundary (see above) $\Gamma_R = \partial B(\bar{x}, R)$ and the perforated domain $\mathcal{O}_\rho = \mathcal{O} \setminus (\bar{x} + (\rho\omega_1 \cup (\delta\mathbf{e} + \rho\omega_2)))$. Also let u_ρ be the solution to the Poisson equation on $\mathcal{O}_\rho$ with free Neumann conditions on the boundaries of the holes. Then we have the following statement giving an asymptotic expansion of the cost function with respect to ρ:

Theorem 1. *Let $j(\rho) = J(u_\rho)$ be a cost function where J does not explicitly depend on ρ and $DJ(u)$ is continuous and linear on $\mathcal{V}_R = \{u \in H^1(\mathcal{O}_R), u = 0 \text{ on } \Gamma_R\}$. Let $v_0 \in \mathcal{V}_R$ be the solution to the adjoint equation*

$$a_0(w, v_0) = -DJ(u_0)w \quad \forall w \in \mathcal{V}_R,$$

and let

$$\mathfrak{d}^{(1)}_{topo} := \int_{\Gamma_R} \nabla_x \left(S^{(1),1}_{\omega_1}(x, \nabla u_0(\bar{x})) + S^{(1),1}_{\omega_2}(x, \nabla u_0(\bar{x})) \right) \mathbf{n}(x) v_0(x) \, \mathrm{d}\gamma(x)$$

$$\mathfrak{d}^{(1)}_{int,1} := \int_{\Gamma_R} \nabla_x \left(\widetilde{S}^{(1),1}_{\omega_1}(x, \nabla u_0(\bar{x})) + \widetilde{S}^{(1),1}_{\omega_2}(x, \nabla u_0(\bar{x})) \right) \mathbf{n}(x) v_0(x) \, \mathrm{d}\gamma(x)$$

$$\mathfrak{d}^{(1)}_{int,2} := \int_{\Gamma_R} \nabla_x \left(\widehat{S}^{(1),1}_{\omega_1}(x, \nabla^2 u_0(\bar{x})) + \widehat{S}^{(1),1}_{\omega_2}(x, \nabla^2 u_0(\bar{x})) \right) \mathbf{n}(x) v_0(x) \, \mathrm{d}\gamma(x)$$

$$+ \int_{\Gamma_R} \mathbf{e}\nabla^2_x \left(S^{(1),1}_{\omega_2}(x, \nabla u_0(\bar{x})) \right) \mathbf{n}(x) v_0(x) \, \mathrm{d}\gamma(x)$$

$$\mathfrak{d}^{(2)}_{topo} := \int_{\Gamma_R} \nabla_x \left(S^{(1),2}_{\omega_1}(x, \nabla u_0(\bar{x})) + S^{(2),1}_{\omega_1}(x, \nabla^2 u_0(\bar{x})) \right) \mathbf{n}(x) v_0(x) \, \mathrm{d}\gamma(x)$$

$$+ \int_{\Gamma_R} \nabla_x \left(S^{(1),2}_{\omega_2}(x, \nabla u_0(\bar{x})) + S^{(2),1}_{\omega_2}(x, \nabla^2 u_0(\bar{x})) \right) \mathbf{n}(x) v_0(x) \, \mathrm{d}\gamma(x).$$

Then the function has the following asymptotic expansion:

$$j(\rho) = j(0) + \left\{ \mathfrak{d}^{(1)}_{topo} + \left(\frac{\rho}{\delta}\right)^n \mathfrak{d}^{(1)}_{int,1} + \delta \mathfrak{d}^{(1)}_{int,2} \right\} \rho^n + \left\{ \mathfrak{d}^{(2)}_{topo} \right\} \rho^{n+1} + o\left(\rho^{n+1}\right).$$

Here we assume that $\delta = \rho^\alpha$, with $\alpha \in (\frac{1}{2}, \frac{3}{4})$.

The terms $S^{(i),j}_{\omega_k}$, $\widetilde{S}^{(i),j}_{\omega_k}$ and $\widehat{S}^{(i),j}_{\omega_k}$ are based on approximations of single layer potentials associated to exterior Neumann problems, reflecting the behaviour of the inner problem. In particular, the terms in $\mathfrak{d}^{(1)}_{topo}$ are the same that appear when computing the topological derivative for each individual hole (see also [61]) and the terms in $\mathfrak{d}^{(2)}_{topo}$ are reflecting the second order topological derivatives of each hole. The interaction is described by $\mathfrak{d}^{(1)}_{int,1}$ and $\mathfrak{d}^{(1)}_{int,2}$. Here, $\mathfrak{d}^{(1)}_{int,1}$ is the first expansion term (with respect to the scaling parameter $\left(\frac{\rho}{\delta}\right)$) approximating the interaction between two holes in the aforementioned exterior Neumann problem. On the other hand, $\mathfrak{d}^{(1)}_{int,2}$ is the leading order correction term for the fact that the topology derivative for ω_2 should be computed at $\bar{x} + \delta$ but is instead computed only in $\bar{x}$.

Outlook: a reduced model for the optimization of perforated geometries. Theorem 1 gives an explicit expression for the hole-hole interaction in the topological derivative. Controlling the pairwise interaction permits to obtain in a natural way an estimate for the interaction terms in a lattice of holes, as was indicated in (27) and in Figure 16(a). Indeed, much as in atomic lattices, one can approximate the total energy of the lattice by the sum of the pairwise interactions of neighbours. This strategy will permit us to estimate the influence of lattice-like microstructures on the objective functional, either in a single-scale approach as in Section 6 or in a two-scale approach where hole structures of ellipses on a periodic lattice are used to describe microstructures. This class of microstructures is markedly different from the laminates typically used in two-scale shape optimization [3]. It remains an open problem to understand if this difference in the microstructure will result in a significant difference at the macroscopic level.

References

[1] ADALI, S., J.C. BRUCH, J., SADEK, I., AND SLOSS, J. Robust shape control of beams with load uncertainties by optimally placed piezo actuators. *Structural and Multidisciplinary Optimization 19*, 4 (2000), 274–281.

[2] ALBERS, S. Online algorithms: a survey. *Mathematical Programming 97* (2003), 3–26.

[3] ALLAIRE, G. *Shape Optimization by the Homogenization Method*, vol. 146. Springer Applied Mathematical Sciences, 2002.

[4] ALLAIRE, G., BONNETIER, E., FRANCFORT, G., AND JOUVE, F. Shape optimization by the homogenization method. *Numerische Mathematik 76* (1997), 27 – 68.

[5] ALLAIRE, G., DE GOURNAY, F., JOUVE, F., AND TOADER, A.-M. Structural optimization using topological and shape sensitivity via a level set method. *Control and Cybernetics 34* (2005), 59–80.

[6] ALLAIRE, G., AND JOUVE, F. A level-set method for vibration and multiple loads structural optimization. *Comput. Methods Appl. Mech. Engrg. 194*, 30-33 (2005), 3269–3290.

[7] ALLAIRE, G., JOUVE, F., AND DE GOURNAY, F. Shape and topology optimization of the robust compliance via the level set method. *ESAIM Control Optim. Calc. Var. 14* (2008), 43–70.

[8] ALLAIRE, G., JOUVE, F., AND TOADER, A.-M. Structural optimization using sensitivity analysis and a level-set method. *Journal of Computational Physics 194*, 1 (2004), 363–393.

[9] ALVAREZ, F., AND CARRASCO, M. Minimization of the expected compliance as an alternative approach to multiload truss optimization. *Struct. Multidiscip. Optim. 29* (2005), 470–476.

[10] AMSTUTZ, S., AND ANDRÄ, H. A new algorithm for topology optimization using a level-set method. *Journal of Computational Physics 216* (2006), 573–588.

[11] ATWAL, P. Continuum limit of a double-chain model for multiload shape optimization. *Journal of Convex Analysis 18*, 1 (2011).

[12] BANICHUK, N. V., AND NEITTAANMÄKI, P. On structural optimization with incomplete information. *Mechanics Based Design of Structures and Machines 35* (2007), 75–95.

[13] BASTIN, F., CIRILLO, C., AND TOINT, P. Convergence theory for nonconvex stochastic programming with an application to mixed logit. *Math. Program. 108* (2006), 207–234.

[14] BEN-TAL, A., EL-GHAOUI, L., AND NEMIROVSKI, A. *Robust Optimization*. Princeton University Press, Princeton and Oxford, 2009.

[15] BEN-TAL, A., KOČVARA, M., NEMIROVSKI, A., AND ZOWE, J. Free material design via semidefinite programming: the multiload case with contact conditions. *SIAM J. Optim. 9* (1999), 813–832.

[16] BENDSØE, M. P. *Optimization of structural topology, shape, and material*. Springer-Verlag, Berlin, 1995.

[17] BURGER, M., HACKL, B., AND RING, W. Incorporating topological derivatives into level set methods. *J. Comp. Phys. 194* (2004), 344–362.

[18] BURGER, M., AND OSHER, S. J. A survey on level set methods for inverse problems and optimal design. *European Journal of Applied Mathematics 16*, 2 (2005), 263–301.

[19] CHANG, F. R. *Stochastic Optimization in Continuous Time*. Cambridge University Press, Cambridge, 2004.

[20] CHERKAEV, A., AND CHERKAEV, E. Stable optimal design for uncertain loading conditions. In *Homogenization*, V. B. et al., Ed., vol. 50 of *Series on Advances in Mathematics for Applied Sciences*. World Scientific, Singapore, 1999, pp. 193–213.

[21] CHERKAEV, A., AND CHERKAEV, E. Principal compliance and robust optimal design. *Journal of Elasticity 72* (2003), 71–98.

[22] CIARLET, P. G. *Mathematical Elasticity Volume I: Three-Dimensional Elasticity*, vol. 20. Studies in Mathematics and its Applications, North-Holland, 1988.

[23] CLEMENTS, D., AND RIZZO, F. A Method for the Numerical Solution of Boundary Value Problems Governed by Second-order Elliptic Systems. *IMA Journal of Applied Mathematics 22* (1978), 197–202.

[24] CONTI, S., HELD, H., PACH, M., RUMPF, M., AND SCHULTZ, R. Risk averse shape optimization. *Siam Journal on Control and Optimization* (2009). submitted.

[25] Conti, S., Held, H., Pach, M., Rumpf, M., and Schultz, R. Shape optimization under uncertainty – a stochastic programming perspective. *SIAM J. Optim. 19* (2009), 1610–1632.

[26] de Gournay, F., Allaire, G., and Jouve, F. Shape and topology optimization of the robust compliance via the level set method. *ESAIM: Control, Optimisation and Calculus of Variations 14* (2007), 43–70.

[27] Delfour, M. C., and Zolésio, J. *Geometries and Shapes: Analysis, Differential Calculus and Optimization.* Adv. Des. Control 4. SIAM, Philadelphia, 2001.

[28] Dias, G. P., Herskovits, J., and Rochinha, F. A. Simultaneous shape optimization and nonlinear analysis of elastic solids. *Computational Mechanics* (1998).

[29] Du, Q., and Wang, D. Tetrahedral mesh generation and optimization based on centroidal Voronoi tesselations. *International Journal for Numerical Methods in Engineering 56* (2003), 1355–1373.

[30] Fleming, W. H., and Rishel, R. W. *Deterministic and Stochastic Optimal Control.* Springer, New York, 1975.

[31] Garreau, S., Guillaume, P., and Masmoudi, M. The topological asymptotic for PDE systems: The elasticity case. *SIAM J. Control Optim. 39*, 6 (2001), 1756–1778.

[32] Guedes, J. M., Rodrigues, H. C., and Bendsøe, M. P. A material optimization model to approximate energy bounds for cellular materials under multiload conditions. *Struct. Multidiscip. Optim. 25* (2003), 446–452.

[33] Hackbusch, W. *Integral Equations*, vol. 120 of *International Series of Numerical Mathematics.* Birkhäuser Verlag, Basel, Boston, Berlin, 1995.

[34] Hackbusch, W., and Sauter, S. Composite finite elements for the approximation of PDEs on domains with complicated micro-structures. *Numerische Mathematik 75* (1997), 447–472.

[35] He, L., Kao, C.-Y., and Osher, S. Incorporating topological derivatives into shape derivatives based level set methods. *Journal of Computational Physics 225*, 1 (2007), 891–909.

[36] Huyse, L. *Free-form airfoil shape optimization under uncertainty using maximum expected value and second-order second-moment strategies.* ICASE report ; no. 2001-18. ICASE, NASA Langley Research Center Available from NASA Center for Aerospace Information, Hampton, VA, 2001.

[37] Liehr, F., Preusser, T., Rumpf, M., Sauter, S., and Schwen, L. O. Composite finite elements for 3D image based computing. *Computing and Visualization in Science 12* (2009), 171–188.

[38] Liu, Z., Korvink, J. G., and Huang, R. Structure topology optimization: Fully coupled level set method via femlab. *Structural and Multidisciplinary Optimization 29* (June 2005), 407 – 417.

[39] Marsden, J., and Hughes, T. *Mathematical foundations of elasticity.* Dover Publications Inc., New York, 1993.

[40] Marti, K. *Stochastic Optimization Methods.* Springer, Berlin, 2005.

[41] Melchers, R. Optimality-criteria-based probabilistic structural design. *Structural and Multidisciplinary Optimization 23*, 1 (2001), 34–39.

[42] Osher, S., and Fedkiw, R. *Level Set Methods and Dynamic Implicit Surfaces*, vol. 153. Applied Mathematical Sciences, Springer, 2003.

[43] Osher, S. J., and Sethian, J. A. Fronts propagating with curvature dependent speed: algorithms based on hamilton-jacobi formulations. *Journal of Computational Physics 79* (1988), 12–49.

[44] Owen, S. J. A survey of unstructured mesh generation technology. In *Proceedings of the 7th International Meshing Roundtable* (Dearborn, Michigan, 1998), Sandia National Laboratories, pp. 239–267.

[45] Pach, M. *Levelsetverfahren in der Shapeoptimierung.* University of Duisburg-Essen, 2005. Diploma thesis, available here: `http://www.uni-duisburg.de/FB11/disma/m_pach/ShapeOpt.pdf`.

[46] Pennanen, T. Epi-convergent discretizations of multistage stochastic programs. *Mathematics of Operations Research 30* (2005), 245–256.

[47] Pflug, G. C., and Römisch, W. *Modeling, Measuring and Managing Risk.* World Scientific, Singapore, 2007.

[48] Rumigny, N., Papadopoulos, P., and Polak, E. On the use of consistent approximations in boundary element-based shape optimization in the presence of uncertainty. *Comput. Methods Appl. Mech. Engrg. 196* (2007), 3999–4010.

[49] Ruszczyński, A., and Shapiro, A., Eds. *Handbooks in Operations Research and Management Sciences, 10: Stochastic Programming.* Elsevier, Amsterdam, 2003.

[50] Schultz, R. Stochastic programming with integer variables. *Mathematical Programming 97* (2003), 285–309.

[51] SCHULTZ, R., AND TIEDEMANN, S. Risk aversion via excess probabilities in stochastic programs with mixed-integer recourse. *SIAM J. on Optimization 14*, 1 (2003), 115–138.

[52] SCHULZ, V., AND SCHILLINGS, C. On the nature and treatment of uncertainties in aerodynamic design. *AIAA Journal 47* (2009), 646–654.

[53] SCHUMACHER, A. *Topologieoptimierung von Bauteilstrukturen unter Verwendung von Lochpositionierungskriterien.* PhD thesis, Universität – Gesamthochschule Siegen, 1996.

[54] SETHIAN, J. A. *Level Set Methods and Fast Marching Methods.* Cambridge University Press, 1999.

[55] SETHIAN, J. A., AND WIEGMANN, A. Structural boundary design via level set and immersed interface methods. *Journal of Computational Physics 163*, 2 (2000), 489 – 528.

[56] SHAPIRO, A., DENTCHEVA, D., AND RUSZCZYŃSKI, A. *Lectures on Stochastic Programming.* SIAM-MPS, Philadelphia, 2009.

[57] SHEWCHUK, J. Triangle: Engineering a 2d quality mesh generator and delaunay triangulator. *Applied Computational Geometry: Towards Geometric Engineering 1148* (1996), 203–222.

[58] SHEWCHUK, J. Delaunay refinement algorithms for triangular mesh generation. *Computational Geometry: Theory and Applications 22* (2002), 21–74.

[59] SOKOŁOWSKI, J., AND ŻOCHOWSKI, A. On the topological derivative in shape optimization. *SIAM J. Control Optim. 37*, 4 (1999), 1251–1272.

[60] SOKOŁOWSKI, J., AND ŻOCHOWSKI, A. Topological derivatives of shape functionals for elasticity systems. *Mech. Struct. & Mach. 29*, 3 (2001), 331–349.

[61] SOKOŁOWSKI, J., AND ŻOCHOWSKI, A. Optimality conditions for simultaneous topology and shape optimization. *SIAM Journal on Control and Optimization 42*, 4 (2003), 1198–1221.

[62] SOKOŁOWSKI, J., AND ZOLÉSIO, J.-P. *Introduction to Shape Optimization: Shape Sensitivity Analysis.* Springer, 1992.

[63] STEINBACH, M. Tree-sparse convex programs. *Mathematical Methods of Operations Research 56* (2002), 347–376.

[64] WÄCHTER, A. *An Interior Point Algorithm for Large-Scale Nonlinear Optimization with Applications in Process Engineering.* Phd thesis, Carnegie Mellon University, 2002.

[65] WÄCHTER, A., AND BIEGLER, L. On the implementation of a primal-dual interior point filter line search algorithm for large-scale nonlinear programming. *Mathematical Programming 106*, 1 (2006), 25–57.

[66] ZHUANG, C., XIONG, Z., AND DING, H. A level set method for topology optimization of heat conduction problem under multiple load cases. *Comput. Methods Appl. Mech. Engrg. 196* (2007), 1074–1084.

Pradeep Atwal
Institut für Angewandte Mathematik
Universität Bonn
Endenicher Allee 60
53115 Bonn
Germany
e-mail: `pradeep.atwal@uni-bonn.de`

Sergio Conti
Institut für Angewandte Mathematik
Universität Bonn
Endenicher Allee 60
53115 Bonn
Germany
e-mail: `sergio.conti@uni-bonn.de`

Benedict Geihe
Institut für Numerische Simulation
Universität Bonn
Endenicher Allee 60
53115 Bonn
Germany
e-mail: `benedict.geihe@ins.uni-bonn.de`

Martin Pach
Fakultät für Mathematik
Universität Duisburg-Essen
Forsthausweg 2
D-47057 Duisburg
Germany
e-mail: `pach@math.uni-duisburg.de`

Martin Rumpf
Institut für Numerische Simulation
Universität Bonn
Endenicher Allee 60
53115 Bonn
Germany
e-mail: `martin.rumpf@ins.uni-bonn.de`

Rüdiger Schultz
Fakultät für Mathematik
Universität Duisburg-Essen
Forsthausweg 2
D-47057 Duisburg
Germany
e-mail: `schultz@math.uni-duisburg.de`